Production cross sections of elements near the N=126 shell in ^{48}Ca-induced reactions with ^{154}Gd,^{159}Tb,^{162}Dy, and ^{165}Ho targets

D. A. Mayorov, T. A. Werke, M. C. Alfonso, M. E. Bennett, and C. M. Folden, III

Phys. Rev. C **90**, 024602 — Published 4 August 2014

DOI: 10.1103/PhysRevC.90.024602

Production cross sections of elements near the $N = 126$ shell in ^{48}Ca-induced reactions with ^{154}Gd, ^{159}Tb, ^{162}Dy and ^{165}Ho targets

D. A. Mayorov[1,2], T. A. Werke[1,2], M. C. Alfonso[1,2], M. E. Bennett[1,*], C. M. Folden III[1,†]

[1]*Cyclotron Institute, Texas A&M University, College Station, Texas 77843, USA*

[2]*Department of Chemistry, Texas A&M University, College Station, Texas 77843, USA*

Excitation functions for shell-stabilized evaporation residues produced in ^{48}Ca-induced reactions with ^{154}Gd, ^{159}Tb, ^{162}Dy, and ^{165}Ho targets have been measured in experiments performed at the Cyclotron Institute at Texas A&M University. The examined energy range predominantly covers the 3*n* and 4*n* evaporation channels, with higher cross sections measured for the 4*n* products. The σ_{4n} are nearly invariant within experimental uncertainty in reactions with ^{159}Tb, ^{162}Dy, and ^{165}Ho with the maxima at 12.6 ± 1.9 mb, 12.6 ± 1.7 mb, and 9.4 ± 1.3 mb, respectively. For the reaction with ^{154}Gd, the maximum is slightly lower at 4.0 ± 0.6 mb. A simple model to describe the measured production cross sections was employed. Capture was estimated using the "diffused barrier formula" from the "fusion by diffusion" model proposed by Świątecki *et al*. The fusion probability was estimated using a phenomenological expression presented by Siwek-Wilczyńska *et al*. The survival probability was calculated according to the formula of Vandenbosch and Huizenga, derived from transition-state theory. Best agreement is reached between calculation and experiment upon inclusion of collective effects in the calculation of the survival probability, shown previously to be important for production of weakly deformed nuclei. This, in turn, challenges the expectation of strong shell-stabilization benefiting the production cross section. The present data is compared with earlier studies on production of neutron-deficient nuclei in Ca-induced reactions with lanthanide targets.

PACS number(s): 25.70.Gh, 25.70.Jj

[*] Present Address: Division of Chemical Sciences and Engineering, Argonne National Laboratory, Argonne, Illinois 60439, USA.

[†] Corresponding author. Email Address: Folden@comp.tamu.edu

I. INTRODUCTION

The landscape of nuclides above the $Z = 82$ shell and near the $N = 126$ shell provides an excellent laboratory to investigate the production cross sections of fusion-evaporation residues, since nuclei of largely varying fissility, nucleon binding energy, and deformation populate the region. These nuclei can be formed by the fusion of a medium-mass projectile with a moderately heavy target to form an excited compound nucleus that decays predominantly by neutron emission, charged particle emission, or fission. Andreyev *et al*. studied the production of very neutron-deficient isotopes of Bi and Po (see [1] and references therein) and At [2], and compared their data to model calculations. These researchers found a need to reduce the theoretical fission barrier [3] by ≤35% in order to agreeably describe the measured *xn* and *pxn* cross sections. Moreover, the yield of *xn* channels was substantially reduced due to significant competition from *pxn* channels. For more neutron-rich nuclei, proton emission is not as significant and a larger fission barrier is expected to lead to enhancement of the production cross section. However, when Vermeulen *et al.* [4] used ^{40}Ar-induced reactions to study the production of shell-stabilized nuclides near the $N = 126$ shell, they had to substantially reduce the spherical shell effects applied in model calculations to obtain good agreement with their data. Similar observations were made by Sahm *et al.* [5] in reactions between ^{48}Ca and isotopes of Yb that produced excited $^{224, 221, 220}$Th nuclei. This unexpected wash-out of shell effects at quite low excitation energies was attributed to enhancement of the nuclear level density by collective degrees of freedom, which overcome any shell-stabilizing effects on the production cross section. The resulting collective enhancement of level density (CELD) gains significance as a spherical nucleus approaches the saddle configuration due to the appearance of rotational bands, and increases the probability that an excited nucleus formed in fusion will fission [6-8]. CELD may also affect superheavy (SH) element formation, since modern-day efforts to synthesize elements with $Z > 118$ [9-12] approach predicted spherical shells beyond those known at $Z = 82$ and $N = 126$. In the present work we investigate the production of heavy elements in the vicinity of the closed shells at $Z = 82$, $N = 126$ synthesized in ^{48}Ca-induced reactions with ^{154}Gd, ^{159}Tb, ^{162}Dy, and ^{165}Ho targets. The products of these reactions are roughly between the Bi, Po, and At residues studied by Andreyev *et al*. and the Th residues studied by Sahm *et al*., thus expanding the available experimental data for production cross sections of spherical, neutron-deficient nuclides. These

data are also part of a larger systematic study involving reactions between projectiles with $Z \geq 20$ and lanthanide targets, and preliminary results were reported in [13].

II. EXPERIMENTAL METHODS

The experimental data were collected at the Cyclotron Institute at Texas A&M University, utilizing the Momentum Achromat Recoil Spectrometer (MARS) [14]. The experimental setup is shown in Fig. 1 and is substantially similar to that described in [15], so only the most important details are presented here. Beams of $^{48}Ca^{5+}$ or $^{48}Ca^{7+}$ (≈5 MeV/u of intensity 1 – 10 pnA) were delivered by the K500 cyclotron for irradiation of ^{154}Gd (1.0 mg/cm^2 $^{154}Gd_2O_3$ on 2 μm Ti), ^{159}Tb (497 μg/cm^2 self-supporting), ^{162}Dy (403 μg/cm^2 on 75 μg/cm^2 ^{nat}C), and ^{165}Ho (498 μg/cm^2 self-supporting) targets, in three temporally separated experiments. The ^{154}Gd target, enriched to >95% in ^{154}Gd, was prepared onsite by molecular plating of the nitrate salt on a ^{nat}Ti backing foil [16]. The ^{159}Tb and ^{165}Ho targets were prepared by rolling and purchased from Microfoils Co., and the ^{162}Dy target was prepared by vacuum deposition. The beam dose on target was monitored by two collimated ion-implanted Si detectors positioned at ±30^o to the beam axis. To reduce transmission of unwanted scattered particles seen by the Si monitors, a plastic cylindrical blocker 21.6 mm in length and with a center opening 6.35 mm in diameter was added ahead of each collimator. An electron-suppressed Faraday cup, placed downstream of the target position, was used to calibrate the absolute beam dose. The beam energy was varied using 0 (no degrader), 1.20, 2.25, 2.85, 3.45, 4.50, 5.10, and 6.29 μm Al degraders for the excitation function measurements. The energy of the beam was determined to an accuracy of 1% by passing the primary beam through a ^{nat}C foil (≈50 μg/cm^2) and measuring the magnetic rigidity of the stripped beam charge states after dipole magnet D1. The ^{nat}C foil was also used for charge equilibration of the evaporation residues (EvRs). All energy losses in this work were calculated using LISE++ [17] according to the method of Ziegler *et al*. [18].

Reaction products were separated from primary beam based on their differing magnetic rigidity and velocity. For each EvR of interest, the separator was tuned for the most probable charge state as estimated according to Schiwietz and Grande [19]. The transmission efficiency of MARS was previously investigated for products of the ^{40}Ar + ^{165}Ho reaction [15], calculated as a global fit of the ratio of our measured product rates to literature data of Andreev *et al.* [2] for a series of *xn* and *pxn* excitation functions. The resulting efficiency for that reaction was ε_{MARS} =

(0.9 ± 0.1)%. Since then, measurements of beam intensity by the electron-suppressed Faraday cup (located directly in the target chamber) uncovered a systematic offset in the previous beam dose data. After necessary corrections, the recalculated efficiency for the ^{40}Ar + ^{165}Ho reactions is ε_{MARS} = (2.2 ± 0.5)%. The efficiency for transmission of EvRs in the more symmetric reaction ^{118}Sn(^{40}Ar, 6*n*)^{152}Er was determined to be ε_{MARS} = (3.5 ± 0.7)%. ε_{MARS} is in the range (2.9 ± 0.7)% – (3.2 ± 0.8)% for the *xn* residues of the present ^{48}Ca reactions, interpolated as a function of the mass asymmetry η between the experimental results for the ^{40}Ar-induced reactions. η is defined as $|A_P - A_T|/(A_P + A_T)$, where the *P* and *T* subscripts represent the projectile and target, respectively.

The transmitted products were detected by an X1 design 16-strip position-sensitive silicon detector (PSSD) with an active area of 50 x 50 mm purchased from Micron Semiconductor Ltd. The PSSD energy calibration was obtained using a four-peak α-source containing a mixed sample of ^{148}Gd, ^{239}Pu, ^{241}Am, and ^{244}Cm, each with an activity of ≈10 nCi. An aluminum mask with multiple horizontal slits 1 mm in width and spaced 8 mm apart vertically was used to obtain a calibration for vertical position in each of the 16 strips. The position resolution of these detectors is discussed in [15]. For the internal calibration (correction for daughter recoil energy), products of the ^{48}Ca + ^{106}Pd (587 μg/cm^2) reaction were used.

Beam pulsing was employed in all experiments except for those involving the ^{154}Gd target. The beam on/off periods were each 500 ms long, so the probability of observing an α-decay of the implanted EvR in either window was ≈50%, since the EvR half-lives are much greater than 500 ms in all cases. In the ^{154}Gd irradiations, a micro-channel plate (MCP) detector was located upstream of the PSSD and the beam was *not* pulsed. Coincident signals in the two detectors would indicate an implantation event, while a signal in the PSSD alone would indicate a radioactive decay. The electrostatic grid of the MCP that directs electrons toward the detector had a transmission efficiency of ≈85%, whereas the MCP efficiency was >99%. In all experiments, the geometric efficiency of the focal plane PSSD for α-particles emitted into the detector was estimated to be (55 ± 3)%, while the fraction of the EvR spatial distributions striking the detector were (100 ± 2)% in the horizontal direction and ≈(95 ± 5)% in the vertical direction. Data acquisition live time was calculated using a 1 MHz clock signal that was vetoed when the system was busy.

III. RESULTS

Peak-fitting was done with the GF3 program, which is part of the RadWare package [20]. In the pulsed-beam experiments, the beam-off spectra were used to determine the number of decays of each product. In the non-pulsed experiments, the spectra of events not vetoed by a coincident MCP signal were used to determine the number of decays of each product. The products were identified according to their well-known α-energies [21]. Fig. 2 shows typical α-decay spectra collected for the implanted EvRs of each ^{48}Ca-induced reaction studied in the present work. The associated laboratory-frame center-of-target energy ($E_{lab,cot}$) in Fig. 2 corresponds to approximately the excitation function maxima for the respective 4*n* residue. A minor event count correction was made for reaction products with α-decay energies in the range 5.8 – 6.2 MeV due to a contamination background in the detector chamber (1 – 6 h^{-1}).

Particular attention is given to the 3*n* and 4*n* evaporation channels, which typically have the highest cross sections in warm-fusion reactions. Table I lists the decay properties of EvRs produced via these evaporation channels for each ^{48}Ca reaction. The observed decay energies are in good agreement with literature data. Evaporation residue cross sections for all observed *xn* evaporation channels are listed in Table II, with error bars calculated according to [22] at a 1σ level. These errors are statistical only. The absolute uncertainty is estimated to be ±50%, primarily from systematic uncertainty in the transmission of MARS. In Fig. 3, the same data are shown, along with model calculations (see below). Due to the nearly identical half-lives and α-decay energies of the 4*n* and 5*n* evaporation channel products of reactions with ^{162}Dy and ^{165}Ho targets, a sum cross section for the two channels is reported. However, as inferred from the ^{154}Gd and ^{159}Tb reaction data, contribution of the 5*n* channel to the *peak* of the 4*n* excitation function is minimal. Greater error bars for the 3*n* residues from the reaction ^{48}Ca + ^{159}Tb, which have an α-decay branch of (3.91 ± 0.16)% [21], are due to low count statistics. Candidate *pxn* channel events were observed in reactions with ^{162}Dy and ^{165}Ho with low statistics (seen in Figs. 2c and d around 5.9 MeV and 6.1-6.3 MeV, respectively). Cross sections for these *pxn* channels could not be determined reliably due to large uncertainties in determining the contribution from electron-capture decay of *xn* products, long half-lives, and low α-branches. The data suggest that *xn* evaporation is the predominant particle deexctiation mode over the studied excitation energy range. This conclusion is supported by a Monte Carlo cross section calculation [23] for all possible products of each presently studied ^{48}Ca reaction. These calculations indicate that the

largest *pxn* cross sections are expected at the highest examined excitation energies, and the probability of deexcitation by *pxn* evaporation is anticipated to increase with further increases in excitation energy.

IV. MODEL CALCULATIONS

Theoretical models form the backbone for analysis of nuclear reaction data, and relevant models have been extensively discussed in [8, 24-26]. To quantify the impact of the key steps of the fusion-evaporation mechanism on the EvR production cross section, the measured cross section data were modeled by separately calculating the capture cross section σ_{cap} leading to the touching projectile-target configuration, the compound nucleus (CN) formation probability P_{CN} yielding an equilibrated nucleus, and the survival probability W_{xn} for producing a ground-state EvR after deexcitation by emission of x neutrons. The evaporation residue production cross section σ_{xn} can then be estimated by

$$\sigma_{xn} = \sigma_{cap} P_{CN} W_{xn} . \tag{1}$$

Świa□tecki *et al.* [27] developed a semi-empirical formalism for σ_{cap} specific to heavy-ion fusion reactions. The "diffused barrier formula" for capture based on that formalism is

$$\sigma_{cap} = \pi R^2 \frac{\upsilon}{2E_{cm}} \left[X(1+\mathrm{erf}\, X) + \frac{1}{\sqrt{\pi}} \exp(-X^2) \right], \tag{2}$$

$$X = (E_{cm} - B)/\upsilon , \tag{3}$$

where $R = 1.16(A_P^{1/3} + A_T^{1/3})$, E_{cm} is the center-of-mass projectile energy, υ is the Gaussian range parameter, and B is the mean interaction barrier:

$$B = 0.85247z + 0.001361z^2 - 0.00000223z^3 \text{ MeV}. \tag{4}$$

In Eq. (4), z is the Coulomb parameter:

$$z = \frac{Z_P Z_T}{A_P^{1/3} + A_T^{1/3}} , \tag{5}$$

and Z_P, A_P, Z_T, and A_T are the atomic and mass numbers of the projectile and target, respectively. υ is given by

$$\upsilon = CB\sqrt{W_1^2 + W_2^2 + W_0^2} , \tag{6}$$

and considers effects of deformation of the colliding nuclei on the capture process. In Eq. (6), C = 0.07767 fm^{-1}, W_0 = 0.41 fm, and

$$W_i^2 = \frac{R_i^2 \beta_i^2}{4\pi}, \tag{7}$$

where β_i is the quadruple deformation parameter of either the projectile (i = 1) or target (i = 2), and

$$R_i = 1.14 A_i^{1/3} \text{ fm}. \tag{8}$$

For $z \geq 84$, quasifission of the touching configuration reduces fusion, where the fusion cross section for formation of the CN is given by $\sigma_{fus} = \sigma_{cap} P_{CN}$ [28]. Accurate calculation of P_{CN} is the most challenging component of Eq. (1), because it is the least understood process of the fusion-evaporation mechanism [29]. It has been shown that a large deformation of the target nucleus leads to a larger quasifission probability after capture [30]. Since the targets considered here are all well-deformed, inclusion of P_{CN} in the present calculations is necessary. A phenomenological formula describing the dependence of P_{CN} on z was presented by Siwek-Wilczyńska *et al.* [31] and is adapted in this work:

$$P_{CN} = \zeta[10^{-(z/b)^k}], \tag{9}$$

where $k \approx 3.0$, ζ is a scaling parameter introduced in the current work and is described below, and b is an energy-dependent parameter fixed in [31] for 0 MeV and 10 MeV excess kinetic energy above B at b = 135 and b = 155, respectively. The range of compound nucleus excitation energies $E^*_{CN} = E_{cm} + Q$ examined here is ≈35 – 65 MeV. In order to apply Eq. (9) over an extended energy range without a well-established dependence of P_{CN} on E^*_{CN} [29], a simple linear extrapolation of b to account for changes in P_{CN} with E_{cm} was introduced, where

$$b = 2(E_{cm} - B) + 135. \tag{10}$$

The parameterization of Eq. (9) was obtained as a best fit to a series of P_{CN} data extracted using a model-dependent approach. Order of magnitude deviations are observed between the best fit and some of the extracted P_{CN} data, possibly suggesting the need for additional parameters to describe P_{CN} (see [31] for details). For this reason, we include a scaling parameter, ζ, that multiplies the calculated P_{CN} and introduces a systematic shift in the prediction, with a limiting condition of $P_{CN} \leq 1$. In previous studies of ^{48}Ca reacting with lanthanide targets [30, 32], values of P_{CN} in the range 0.3 – 0.8 were reported for $E^*_{CN} \approx 50$ MeV. The choice of ζ in our

calculations was guided by these data: considering only the peak of each 4*n* excitation function measured in the current work, ζ was fixed at 2.5 so that the P_{CN} values would be similar to those previously reported.

The survival probability of an excited compound nucleus by neutron emission (*n*) against fission (*f*) can be expressed in terms of corresponding decay widths Γ_n and Γ_f, respectively, as

$$W_{xn} = P_{xn}(U^*_{CN}) \prod_{i=1}^{x} \left(\frac{\Gamma_n}{\Gamma_n + \Gamma_f} \right)_i = P_{xn}(U^*_{CN}) \prod_{i=1}^{x} \left(\frac{\Gamma_n / \Gamma_f}{1 + \Gamma_n / \Gamma_f} \right)_i , \quad (11)$$

where *i* designates the emitted neutron up to the maximum of *x*, and P_{xn} is the probability that the excited nucleus with thermal excitation energy $U^*_{CN} = E^*_{CN} - E_{rot}$ will emit exactly *x* neutrons [33]. The temperature of a nucleus is $T = \sqrt{U^*_{CN} / a}$. The rotational energy of a nucleus E_{rot} and the level density parameter *a* are defined below. Each emitted neutron is assumed to remove $2\hbar$ units of angular momentum [34] and have kinetic energy $\varepsilon = T$ MeV, which corresponds to the most probable energy assuming a quasi-Maxwellian distribution. It should be noted that in Eq. (11), the possibility of charged-particle emission is neglected. This simplification is made presently for reasons discussed in Section III.

To treat the deexcitation of an excited nucleus with mass number *A* to a nucleus *A–1* via neutron emission, one needs a way to calculate Γ_n and Γ_f. A closed-form expression for Γ_n/Γ_f was derived by Vandenbosch and Huizenga [35], which anticipates differences in the neutron emission and fission level densities through their respective level density parameters a_n and a_f, and is given by

$$\frac{\Gamma_n}{\Gamma_f} = \frac{4K_{coll,n}(A-1)^{2/3} a_f U_n}{K_{coll,f} K_o a_n (2a_f^{1/2} U_f^{1/2} - 1)} \exp(2a_n^{1/2} U_n^{1/2} - 2a_f^{1/2} U_f^{1/2}) , \quad (12)$$

where K_o = 9.8 MeV, K_{coll} is the collective enhancement factor described below, *A* is the mass number of the parent nucleus, and U_n and U_f are the neutron emission and fission thermal energies [24], respectively, defined as

$$U_n = E^*_{CN} - S_n - E_{rot,n} - P_n^{A-1} , \quad (13)$$

$$U_f = E^*_{CN} - B_f - E_{rot,saddle} - P^A_{saddle} , \quad (14)$$

where S_n is the neutron separation energy, $E_{rot,n}$ is the rotational energy after neutron emission, P_n^{A-1} is the pairing energy of the daughter nucleus after neutron emission, B_f is the fission

barrier, $E_{rot,saddle}$ is the rotational energy at the fission saddle, and P^{A}_{saddle} is pairing energy of the parent nucleus at the fission saddle. Neutron separation energies were taken from [21]. The macroscopic component of B_f was calculated according to the rotating finite-range liquid-drop model of Sierk [36] with the ground-state microscopic shell correction to the barrier taken from the tabulated data of M□ller *et al.* [37]. The pairing energy is calculated using $P = 0$ for an odd-odd, δ for an odd-even, or 2δ for an even-even nucleus, where $\delta = 11A^{-1/2}$ MeV. The rotational energy is evaluated assuming a rigid-body moment of inertia $J_{\perp} = \frac{2}{5} m_o A R^2 (1 + \beta_2 / 3)$, where m_o = 931.494 MeV/c^2, β_2 is the quadrupole deformation parameter, and $R = 1.2A^{1/3}$ fm is the nuclear radius. The angular momentum of the CN, l_{CN}, was estimated using the coupled-channel code CCFULL [38], which gives a mean value of l for a given E_{cm}. For a satisfactory description of the experimental excitation function data, l_{CN} had to be reduced by 60%. This limits the l values to < 25$\hbar$, which is consistent with expectations for the EvRs with Z = 84 – 87 [1]. Only low angular momenta should significantly contribute to the yield of *xn* EvRs as a result of the rapid decrease of the liquid-drop (LD) component of B_f, and hence W_{xn}, with increasing l [39].

In Eq. (12) the level density parameters a_n and a_f are modified due to shell effects as prescribed by Ignatyuk *et al.* [40]:

$$a_n = \tilde{a}\left\{1 + \frac{\delta S^{A-1}}{U_n}[1 - \exp(-U_n / d)]\right\}, \tag{15}$$

$$a_f = \tilde{a}\left\{1 + \frac{\delta S^{A}}{U_f}[1 - \exp(-U_f / d)]\right\}, \tag{16}$$

where $\tilde{a}$ is the asymptotic level density parameter, δS^{A-1} and δS^{A} are the shell correction energies of the daughter nucleus and parent nucleus, respectively, and d is the shell damping parameter commonly taken as 18.5 MeV [41]. Shell effects at the saddle point can be neglected, i.e., $\delta S^{A} \approx 0$, therefore Eq. (16) reduces to $a_f = \tilde{a}$ [24]. $\tilde{a}$ was calculated according to the parameterization of Reisdorf [41]:

$$\tilde{a} = 0.04543(r_0 / \text{fm})^3 A + 0.1355(r_0 / \text{fm})^2 A^{2/3} B_S + 0.1426(r_0 / \text{fm}) A^{1/3} B_K, \tag{17}$$

where r_o =1.15 fm, and B_S and B_K are the surface and curvature factors, respectively, tabulated for deformed nuclear shapes in [42]. For spherical nuclei, $B_S = B_K = 1$.

The Vandenbosch-Huizenga formula [Eq. (12)] is based on the Fermi-gas model and the density of levels considers only single-particle nuclear states [35]. Collective states resulting

from nuclear rotation and vibration can enhance the nuclear level density, with this long-range correlation washed-out at higher excitation energies [43]. Collective excitations have been applied to explain the surprisingly low survival probability of weakly deformed excited nuclei produced in fusion reactions, leading to an enhanced fission probability [6, 44]. Here, the formulas of Zagrebaev *et al.* [8] are used to calculate the collective enhancement factor in the fission or neutron emission channel:

$$K_{coll}(U,\beta_2) = K_{rot} f(U) \phi(\beta_2) + K_{vib} f(U) \phi(1-\beta_2), \tag{18}$$

where $\varphi(\beta_2)$ is a smoothing function described below and $f(U)$ represents the damping of collective excitations with increasing excitation energy:

$$f(U) = \left[1 + \exp\left(\frac{U - E_{crit}}{d_{crit}} \right) \right]^{-1}, \tag{19}$$

where the critical energy and width parameters are E_{crit} = 40 MeV and d_{crit} = 10 MeV, respectively, and have been obtained by fitting experimental cross section data [6]. The rotational and vibrational enhancement factors are calculated according to the expressions [23]

$$K_{rot} = \frac{J_{\perp} T}{\hbar^2}, \tag{20}$$

$$K_{vib} = \exp[0.0555 A^{2/3} (T / \mathrm{MeV})^{4/3}]. \tag{21}$$

Typically, $K_{vib} \approx 1 - 10$, while $K_{rot} \approx 100 - 150$ due to the finer level spacing of rotational bands, resulting in a greater level density enhancement. For spherical nuclei, K_{rot} = 1, since rotational bands are forbidden. Therefore, nuclear deformation is an integral component of K_{coll}, and a function of β_2 is introduced that regulates this dependence. The smoothing function $\varphi(\beta_2)$ is

$$\phi(\beta_2) = \left[1 + \exp\left(\frac{\beta_2^0 - |\beta_2|}{\Delta\beta_2} \right) \right]^{-1}, \tag{22}$$

where the transition between spherical and deformed nuclei is defined by the threshold $\beta_2^0 \approx 0.15$ and $\Delta\beta_2 \approx 0.04$. The value of β_2 entering Eq. (22) is either the ground-state quadrupole deformation $\beta_{2,g.s.}$ or the saddle-point quadrupole deformation $\beta_{2,s.p.}$, taken from M□ller *et al.* [37] and Cohen *et al.* [45], respectively.

Eq. (12) relates the thermal energy of an excited system to its decay widths, and the most important term in practice is the exponential term. Changes in Γ_n/Γ_f can be understood

qualitatively as changes in $B_f - S_n$, since S_n and B_f affect Γ_n/Γ_f through Eqs. (13) and (14), respectively. Therefore, changes in W_{xn} can be *qualitatively* understood as changes in the average difference $\overline{B_f - S_n}$ as the excited nucleus progresses through its deexcitation cascade. This insight will help explain the experimental data in Section V.

V. DISCUSSION

As a check of the above model, particularly the credibility of W_{xn}, calculations with and without CELD were performed for the asymmetric reaction ^{188}Os(^{19}F, *xn*)$^{207-x}$At, which produces the same CN as ^{159}Tb(^{48}Ca, *xn*)$^{207-x}$At. The ^{19}F + ^{188}Os reaction was studied by Mahata *et al.* [46], who detected residues by their γ-activity and reported data for the 3*n* – 5*n* evaporation channels. Fig. 4 shows the experimental data as symbols, calculations with CELD as solid lines, and calculations without CELD as dashed lines. Excellent agreement is seen between calculated and literature σ_{cap} data for the ^{19}F-induced reaction. The small value of η for this reaction assures that fusion hindrance plays a minor role in the entrance channel, so P_{CN} is assumed to be close to unity for this system. The satisfactory agreement between the calculation with CELD and the ^{19}F + ^{188}Os experimental data for $E_{lab,cot} < 98$ MeV ($E^*_{CN} < 60$ MeV) suggests that the calculation of the survival probability is reasonable. The ^{48}Ca + ^{159}Tb data are also well-reproduced for the 3*n* and 4*n* excitation functions. The difference in the measured 4*n* excitation function maxima of 60.1 ± 5.1 mb and 12.6 ± 1.9 mb for the ^{19}F- and ^{48}Ca-induced reactions, respectively, can largely be accounted by a 3-to-1 ratio in calculated P_{CN} between the two reactions. Similar ratios of σ_{4n}/σ_{5n} for the two reactions agree roughly with the expectations of the independence postulate [47]; the effect of the Coulomb barrier on the 3*n* cross sections and their larger uncertainties hinders an equivalent conclusion about the σ_{3n}/σ_{4n} ratios. At higher excitation energies, fission delay due to dissipation [48] and pre-equilibrium emission processes can enhance the production cross section, a likely reason for the deviation of the theoretical calculation from the 5*n* EvR experimental data.

The inclusion of CELD helps improve the agreement between theory and experimental data, although the model is very sensitive to changes in its inputs. One important source of uncertainty is the calculation of B_f, since there are no experimental data for the EvRs of the present reactions. The effect of increasing the LD fission barrier by 10% (≈0.8 MeV) relative to

the output of the rotating finite-range liquid-drop model is illustrated by the dashed curves in Fig. 3(d), and increases the calculated cross sections by a factor of 2 – 3. Nonetheless, without any modifications to B_f, the agreement of the model with experimental data is very good, and is owed in large part to inclusion of CELD in the calculation of W_{xn}. EvRs of the ^{48}Ca + ^{154}Gd reaction are most sensitive to CELD as seen from Table III, where the ratio of the maximum production cross section of the 4*n* EvR calculated without and with collective effects is given (σ_{EvR} and $\sigma_{EvR,CELD}$, respectively). These ratios are in close agreement with those obtained from a more sophisticated calculation [23], also shown in Table III. With the smallest $\overline{B_f - S_n}$, the products of the ^{48}Ca + ^{154}Gd reaction have a more pronounced reduction of production cross section due to a larger fission decay width of excited Po isotopes. The less fissile products of the other ^{48}Ca-induced reactions are less sensitive to CELD, since W_{xn} is less sensitive to enhancements of the fission level density when $\Gamma_n >> \Gamma_f$.

The reactions ^{154}Gd(^{48}Ca, *xn*)$^{202-x}$Po and ^{165}Ho(^{48}Ca, *xn*)$^{213-x}$Fr produce nuclides in close proximity to the Z = 82 and N = 126 shells, respectively, and this leads to generally small deformations for the nuclides along the de-excitation cascade. Slightly larger deformations are estimated for nuclides produced in the ^{159}Tb(^{48}Ca, *xn*)$^{207-x}$At and ^{162}Dy(^{48}Ca, *xn*)$^{210-x}$Rn reactions, which are midway between the closed shells. Although subtle, these small differences in β_2 can affect $\varphi(\beta_2)$ and noticeably alter the reduction of σ_{EvR} due to CELD, contributing to the magnitudes of the ratios in the last columns of Table III. However, the link between the ground state deformation and an excited state deformation is not definitively established, so this effect should be interpreted cautiously.

The evidence that large shell-stabilizations do not enhance the production cross sections of spherical nuclei is of consequence to the production of purely shell-stabilized SH nuclei in the vicinity of the predicted spherical shells Z = 120 and N = 184. Modern-day experiments [10-12] aimed at the synthesis of elements with Z > 118 are probing near this SH region of Z and N, with only upper limit cross sections reported so far. Hofman *et al.* [10] investigated the reaction ^{238}U(^{64}Ni, *xn*)$^{302-x}$120 and measured an upper limit cross section of 90 fb. Indications for strong shell-stabilization were not found in their data, which is consistent with the present results for the spherical nuclides near the N = 126 shell. Such a high z (Eq. 5) of the projectile-target pair would also be expected to reduce the production cross section due to a reduced P_{CN}. These phenomena are likely to complicate the search for new elements by substantially reducing the production

cross section below the picobarn level measured for several $Z \leq 118$ transactinides. Some earlier remarks on consequence of CELD to production of SH elements can be found in [6] (and references therein).

The *xn* cross sections in reactions of ^{48}Ca with ^{154}Gd, ^{159}Tb, ^{162}Dy, and ^{165}Ho benefit from reduced competition of *pxn* channels in the deexctiation cascade, a large LD fission barrier of the reactions products, and a relatively small impact of CELD on W_{xn}. On the contrary, a sharp contrast is seen between measured production cross sections of *xn* residues in the fusion reactions ^{159}Tb(^{40}Ca, *xn*)$^{199-x}$At [2] and ^{159}Tb(^{48}Ca, *xn*)$^{207-x}$At. Here the *xn* cross sections are more than three orders of magnitude apart as shown in Fig. 5a. With eight less neutrons, the residues of the ^{40}Ca reactions have a reduced barrier for proton emission and a smaller LD fission barrier. Charged-particle emission from these excited, neutron-deficient residues expels considerable excitation energy, lowering the fission decay width for the remainder of the *xn* deexcitation cascade. This, thereby, results in the higher *pxn* and lower *xn* cross sections.

Fig. 5b shows 4*n* excitation functions for our data and for ^{48}Ca + $^{176,174\text{-}172}$Yb reactions previously reported [5, 49]. The data spans multiple orders of magnitude, and this can be traced to the differences in $\overline{B_f - S_n}$ of the reaction residues. Calculated σ_{cap} for ^{48}Ca + ^{154}Gd, ^{48}Ca + ^{176}Yb, and ^{48}Ca + ^{172}Yb are shown as solid, dashed, and short-dashed curves, respectively, and account but for only a small part of the difference in the *xn* data. For nuclei along the 4*n* deexcitation cascade for reactions with $^{176,174\text{-}172}$Yb targets, $\overline{B_f - S_n}$ = 0.2 MeV, 0.2 MeV, 0.4 MeV, and 0.7 MeV, respectively. The largest cross section in reactions with Yb targets is reported for ^{176}Yb(^{48}Ca, 4*n*)^{220}Th, although its corresponding $\overline{B_f - S_n}$ is one of the lowest. The products of that reaction are also the farthest away from the $N = 126$ shell, with the CN ^{224}Th having $N = 134$. The larger deformations of the heavier Th isotopes produced in reactions with ^{176}Yb likely reduce CELD; the additional rotational levels in a deformed nucleus enhance the level density in the neutron emission channel, compensating for a smaller enhancement in the fission channel. Also of note is the possibility of earlier onset of fission dissipation for mid-closed-shell nuclei relative to closed-shell nuclei as reported by Back *et al.* [48]. With lighter Yb targets, *pxn* channels become more prevalent as the products become more proton-rich, further reducing the *xn* production cross section (this effect was exacerbated for the ^{40}Ca + ^{159}Tb data shown in Fig. 5a).

The complex physics of nuclear deexcitation are evident by the above systematic comparisons and show the importance of minimizing the uncertainties entering theoretical models for a reliable result. Of the aspects discussed in Section IV, the last two terms in the product of Eq. (1) present the greatest challenge in this regard. The nuclear level density is a key ingredient in the calculations of W_{xn}, however the dependence of CELD on excitation energy is still not completely understood. Nonetheless, very satisfactory results were obtained in the description of the measured excitation functions for the ^{48}Ca-induced reactions.

VI. CONCLUSION

The *xn* excitation functions in reactions between ^{48}Ca and targets of ^{154}Gd, ^{159}Tb, ^{162}Dy, and ^{165}Ho have been measured, and a simple model has been employed to explain the data. The model calculations suggest that the competition between neutron emission and fission has the greatest influence on σ_{xn}. The near invariance of the maximum cross sections measured for the 4*n* residues is largely due to similar $\overline{B_f - S_n}$ of the nuclides along the deexcitation cascade. An improved agreement between model estimates and data was found by inclusion of collective enhancement of level density in calculations of the survival probability, consistent with previous literature citing this effect for the production of spherical nuclei. The impact of shell-stabilization on the production cross section is thus suppressed despite the large shell correction energies of the synthesized evaporation residues. The relatively large *xn* cross sections in the current work are attributed to reduced *pxn* competition and large LD fission barriers of the products, which reduce but do not eliminate the impact of collective effects on σ_{xn}.

ACKNOWLEDGEMENTS

The authors would like to thank the Cyclotron Institute accelerator group and technical staff for delivering stable beams of ^{48}Ca. We also thank the Heavy Elements Group at Lawrence Berkeley National Laboratory for providing the ^{162}Dy target and the designs for the molecular plating cell used to fabricate the ^{154}Gd target. One of us (D.A.M.) would like to thank K. Siwek-Wilczyńska and A.V. Karpov for valuable private communications. This work was supported in part by the United States Department of Energy (DOE) under award numbers DE-FG02-

93ER40773 and MUSC09-100, the DOE Early Career Award program under grant number DE-FG02-12ER41869, the Welch Foundation under grant number A-1710, and the Texas A&M University College of Science.

REFERENCES

[1] A. N. Andreyev *et al.*, Phys. Rev. C **72**, 014612 (2005).
[2] A. N. Andreev *et al.*, Sov. J. Nucl. Phys. **52**, 412 (1990).
[3] S. Cohen *et al.*, Ann. Phys. **82**, 557 (1974).
[4] D. Vermeulen *et al.*, Z. Phys. A **318**, 157 (1984).
[5] C. C. Sahm *et al.*, Nucl. Phys. A **441**, 316 (1985).
[6] A. R. Junghans *et al.*, Nucl. Phys. A **629**, 635 (1998).
[7] K.-H. Schmidt *et al.*, Z. Phys. A **315**, 159 (1984).
[8] V. I. Zagrebaev *et al.*, Phys. Rev. C **65**, 014607 (2001).
[9] C. E. Düllman *et al.*, GSI Scientific Report 2011, No. PHN-NUSTAR-SHE-02, edited by K. Große, p. 206.
[10] S. Hofmann *et al.*, GSI Scientific Report 2008, No. NUSTAR-SHE-01, edited by K. Große, p. 131.
[11] J. Khuyagbaatar *et al.*, GSI Scientific Report 2012, No. PHN-ENNA-EXP-01, edited by K. Große, p. 131.
[12] Y. T. Oganessian *et al.*, Phys. Rev. C **79**, 024603 (2009).
[13] C. M. Folden III *et al.*, J. Phys. Conf. Ser. **420**, 012007 (2013).
[14] R. E. Tribble *et al.*, Nucl. Instrum. Methods A **285**, 441 (1989).
[15] C. M. Folden III *et al.*, Nucl. Instrum. Meth. A **678**, 1 (2012).
[16] D. A. Mayorov *et al.*, Cyclotron Institute Progress in Research Report 2013: Heavy Ion Reactions, edited by Y. W. Lui, p. II7.
[17] O. B. Tarasov and D. Bazin, Nucl. Instrum. Methods B **266**, 4657 (2008).
[18] J. F. Ziegler *et al.*, *The Stopping and Range of Ions in Solids* (Pergamon Press, New York, 1984).
[19] G. Schiwietz and P. L. Grande, Nucl. Instrum. Methods B **175**, 125 (2001).
[20] D. C. Radford, RadWare Software Package, http://radware.phy.ornl.gov.
[21] National Nuclear Data Center (2014), http://www.nndc.bnl.gov.
[22] K.-H. Schmidt *et al.*, Z. Phys. A **316**, 19 (1984).
[23] V. I. Zagrebaev *et al.*, Fusion-Evaporation Codes of NRV, http://nrv.jinr.ru/nrv.
[24] K. Siwek-Wilczyńska *et al.*, Phys. Rev. C **72**, 034605 (2005).
[25] W. J. Świa□tecki *et al.*, Phys. Rev. C **78**, 054604 (2008).
[26] V. Weisskopf, Phys. Rev. **52**, 0295 (1937).
[27] W. J. Świa□tecki *et al.*, Phys. Rev. C **71**, 014602 (2005).
[28] A. C. Berriman *et al.*, Nature **413**, 144 (2001).
[29] R. Yanez *et al.*, Phys. Rev. C **88**, 014606 (2013).
[30] G. N. Knyazheva *et al.*, Phys. Rev. C **75**, 064602 (2007).
[31] K. Siwek-Wilczyńska *et al.*, Int. J. Mod. Phys. E **17**, 12 (2008).
[32] R. N. Sagaidak *et al.*, Phys. Rev. C **68**, 014603, 014603 (2003).
[33] J. D. Jackson, Can. J. Phys. **34**, 767 (1956).

[34] F. Plasil and R. L. Ferguson, in *Proceedings of the International Symposium of Physics and Chemistry of Fission* (Vienna: IAEA, Jülich, 1979), p. 521.
[35] R. Vandenbosch and J. Huizenga, *Nuclear Fission* (Academic, New York, 1973), p. 227.
[36] A. J. Sierk, Phys. Rev. C **33**, 2039 (1986).
[37] P. Möller *et al.*, At. Data Nucl. Data Tables **59**, 185 (1995).
[38] K. Hagino *et al.*, Comput. Phys. Commun. **123**, 143 (1999).
[39] K.-H. Schmidt *et al.*, in *Proceedings of the International Symposium on Physics and Chemistry of Fission* (Vienna: IAEA, Jülich, 1979), p. 409.
[40] A. V. Ignatyuk *et al.*, Sov. J. Nucl. Phys, **21**, 255 (1975).
[41] W. Reisdorf, Z. Phys. A **300**, 227 (1981).
[42] W. D. Myers and W. J. Swiatecki, Ann. Phys. **84**, 186 (1974).
[43] P. Roy *et al.*, Phys. Rev. C **88**, 031601 (2013).
[44] A. V. Ignatyuk *et al.*, Sov. J. Nucl. Phys. **37**, 495 (1983).
[45] S. Cohen and W. J. Świa□tecki, Ann. Phys. **22**, 406 (1963).
[46] K. Mahata *et al.*, Nucl. Phys. A **720**, 209 (2003).
[47] S. N. Ghoshal, Phys. Rev. **80**, 938 (1950).
[48] B. B. Back *et al.*, Phys. Rev. C **60**, 044602 (1999).
[49] R. N. Sagaidak *et al.*, JINR FLNR Scientific Report 1997-1998: Heavy Ion Physics, No. E7-2000-232, edited by A. G. Popeko, p. 60.

TABLE I. Decay properties of 3*n* and 4*n* evaporation channel residues produced in the ^{48}Ca-induced reactions in the present work. $E_{\alpha,obs}$ is the observed α-decay energy. The literature data are taken from [21].

Reaction	3*n*, 4*n* EvR	$E_{\alpha,\,obs}$ (keV)	$E_{\alpha,\,lit}$ (keV)	$I_{\alpha,\,lit}$ (%)	$t_{1/2,\,lit}$
^{48}Ca + ^{154}Gd	^{199m}Po	6035.3 ± 1.7	6059.0 ± 3.0	39.0 ± 4.0	4.17 ± 0.05 min
	^{198}Po	6156.1 ± 1.4	6182.0 ± 2.2	57.0 ± 2.0	1.77 ± 0.03 min
^{48}Ca + ^{159}Tb	^{204}At	5950.3 ± 6.7	5950.3 ± 1.3	3.91 ± 0.16	9.22 ± 0.13 min
	^{203}At	6083.4 ± 1.4	6087.0 ± 1.0	31.0 ± 3.0	7.40 ± 0.20 min
^{48}Ca + ^{162}Dy	^{207}Rn	6122.3 ± 4.4	6131.0 ± 4.0	21.0 ± 3.0	9.25 ± 0.17 min
	^{206}Rn	6252.4 ± 3.2[a]	6259.7 ± 1.6	63.0 ± 6.0	5.67 ± 0.17 min
^{48}Ca + ^{165}Ho	^{210}Fr	6542.9 ± 2.7	6545.0 ± 5.0	60.0 ± 30.0	3.18 ± 0.06 min
	^{209}Fr	6649.8 ± 1.4[a]	6646.0 ± 5.0	89.0 ± 3.0	50.5 ± 0.7 s

[a] Reported energy is the combined centroid of 4*n* and 5*n* evaporation channels, since these could not be distinguished with our experimental setup.

TABLE II. Measured production cross sections for the evaporation residues from ^{48}Ca-induced reactions on lanthanide targets studied in this work. $E_{lab,cot}$ is the laboratory-frame center-of-target energy of the projectile.

Reaction	$E_{lab,cot}$ (MeV)	σ_{3n} (mb)	σ_{4n} (mb)	σ_{5n} (mb)	σ_{6n} (mb)
^{48}Ca + ^{154}Gd[a]	185.0	2.1 ± 0.3	0.7 ± 0.1	-	-
	187.8	3.9 ± 0.6	2.1 ± 0.3	-	-
	190.5	2.1 ± 0.4	2.5 ± 0.4	-	-
	196.9	2.4 ± 0.4	4.0 ± 0.6	0.3 ± 0.1	-
	201.5	1.1 ± 0.2	2.9 ± 0.5	1.0 ± 0.2	-
^{48}Ca + ^{159}Tb[b]	185.1	5.1 ± 1.7	3.0 ± 0.6	-	-
	190.8	4.2 ± 3.0	6.1 ± 1.4	-	-
	193.0	3.5 ± 2.0	10.9 ± 1.8	1.5 ± 0.5	-
	193.5	2.5 ± 1.6	12.6 ± 1.9	1.3 ± 0.5	-
	197.8	-	12.5 ± 2.0	1.6 ± 0.7	-
	198.0	-	10.7 ± 1.6	2.7 ± 0.6	-
	201.3	-	7.0 ± 1.1	16.7 ± 4.5	-
	203.1	-	5.8 ± 1.9	17.5 ± 7.0	-
	204.1	-	3.1 ± 0.6	23.3 ± 7.1	-
	209.4	-	2.2 ± 2.0	21.1 ± 7.8	0.8 ± 0.2
^{48}Ca + ^{162}Dy[c]	181.5	1.6 ± 0.4	0.4 ± 0.1		-
	190.2	1.7 ± 0.9	5.7 ± 1.2		-
	197.9	1.3 ± 0.3	12.6 ± 1.7		-
	204.9	0.5 ± 0.2	6.9 ± 1.0		0.3 ± 0.1
	210.4	-	5.4 ± 0.8		1.1 ± 0.2
^{48}Ca + ^{165}Ho[c]	190.8	4.1 ± 0.7	5.5 ± 0.8		-
	193.5	1.5 ± 0.3	9.4 ± 1.3		-
	197.8	0.8 ± 0.2	8.6 ± 1.2		-
	203.1	0.4 ± 0.1	10.2 ± 1.4		-
	209.4	-	11.5 ± 1.6		0.4 ± 0.1

[a] The 3*n* and 5*n* EvRs are the metastable states ^{199m}Po and ^{197m}Po, respectively.

[b] σ_{5n} cross section is the sum for ^{202}At and ^{202m}At.

[c] A sum of the 4*n* and 5*n* channel evaporation residue cross section is reported.

TABLE III. Properties of nuclides produced during the deexcitation cascades. N_{CN} is the compound nucleus neutron number, $\overline{B_f - S_n}$ is the average difference between the ground-state fission barrier B_f (calculated for zero angular momentum) and the neutron separation energy S_n for nuclei encountered in the *xn* deexctiation cascade up to 4*n*, β_2 is the ground-state deformation of the 4*n* EvR, and column 6 and 7 give the ratio of the maximum calculated 4*n* production cross section without and with collective effects (σ_{EvR} and $\sigma_{EvR,CELD}$, respectively). The last column is based on results from a statistical model code [23].

Reaction	4*n* EvR	N_{CN}	$\overline{B_f - S_n}$ (MeV)	β_2(4*n* EvR)	$\sigma_{EvR}/\sigma_{EvR,CELD}$	$\sigma_{EvR}/\sigma_{EvR,CELD}$ [23]
^{48}Ca + ^{154}Gd	^{198}Po	118	4.1	0.000	8.9	6.8
^{48}Ca + ^{159}Tb	^{203}At	122	6.2	0.045	2.9	2.6
^{48}Ca + ^{162}Dy	^{206}Rn	124	6.2	-0.044	3.5	3.3
^{48}Ca + ^{165}Ho	^{209}Fr	126	6.0	-0.044	5.9	4.7

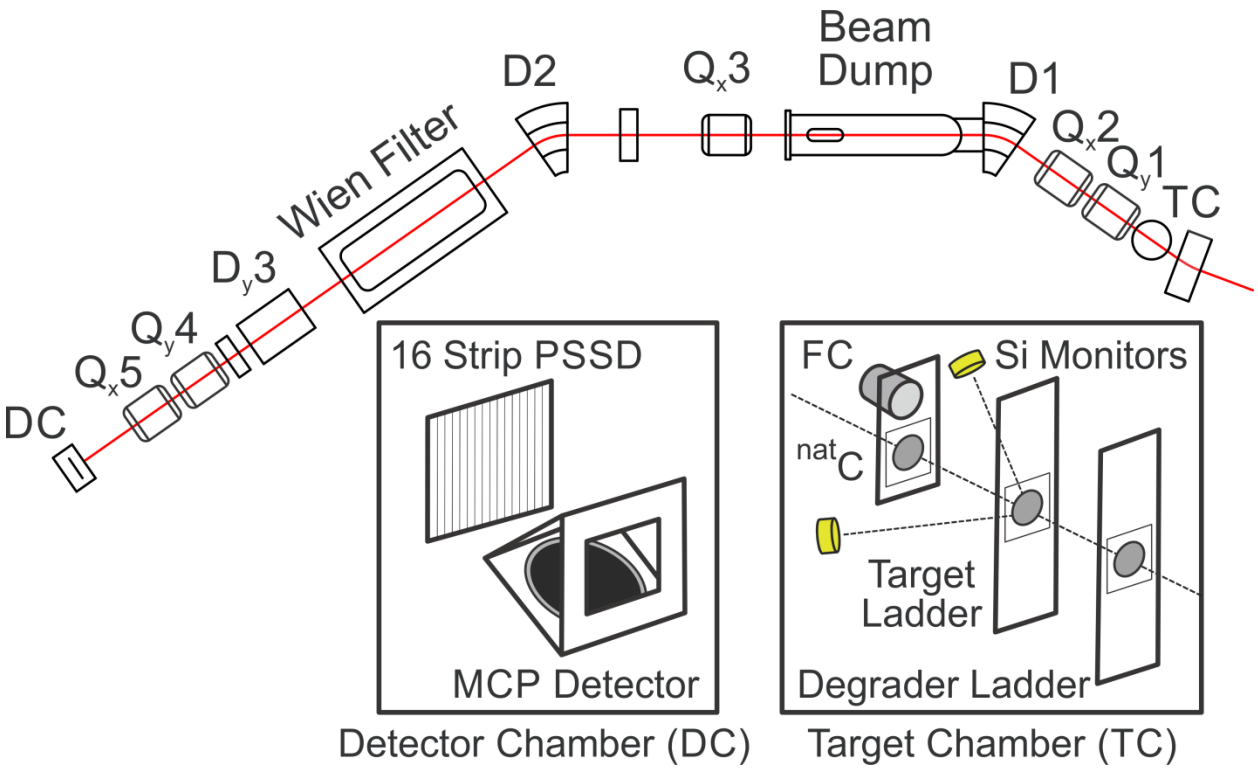

FIG. 1 (Color online) Layout of the experimental setup showing a schematic of the MARS spectrometer. The beam enters from the right of the figure. The target chamber (TC) contains three sets of remotely controlled ladders holding Al degraders, targets, and ^{nat}C foils along with a Faraday cup (FC), in that order. Also, two collimated beam monitor detectors sit at $\pm 30^{o}$ to the beam axis. Dipole and quadrupole magnets are denoted by "D" and "Q," respectively, followed by a number. The bend or focus direction is denoted by the subscript "x" and "y," for horizontal and vertical, respectively. The detector chamber (DC) contains a 16 strip PSSD and an MCP detector, used for implant event and α-decay discrimination. The MCP detector was only used in the ^{154}Gd irradiations.

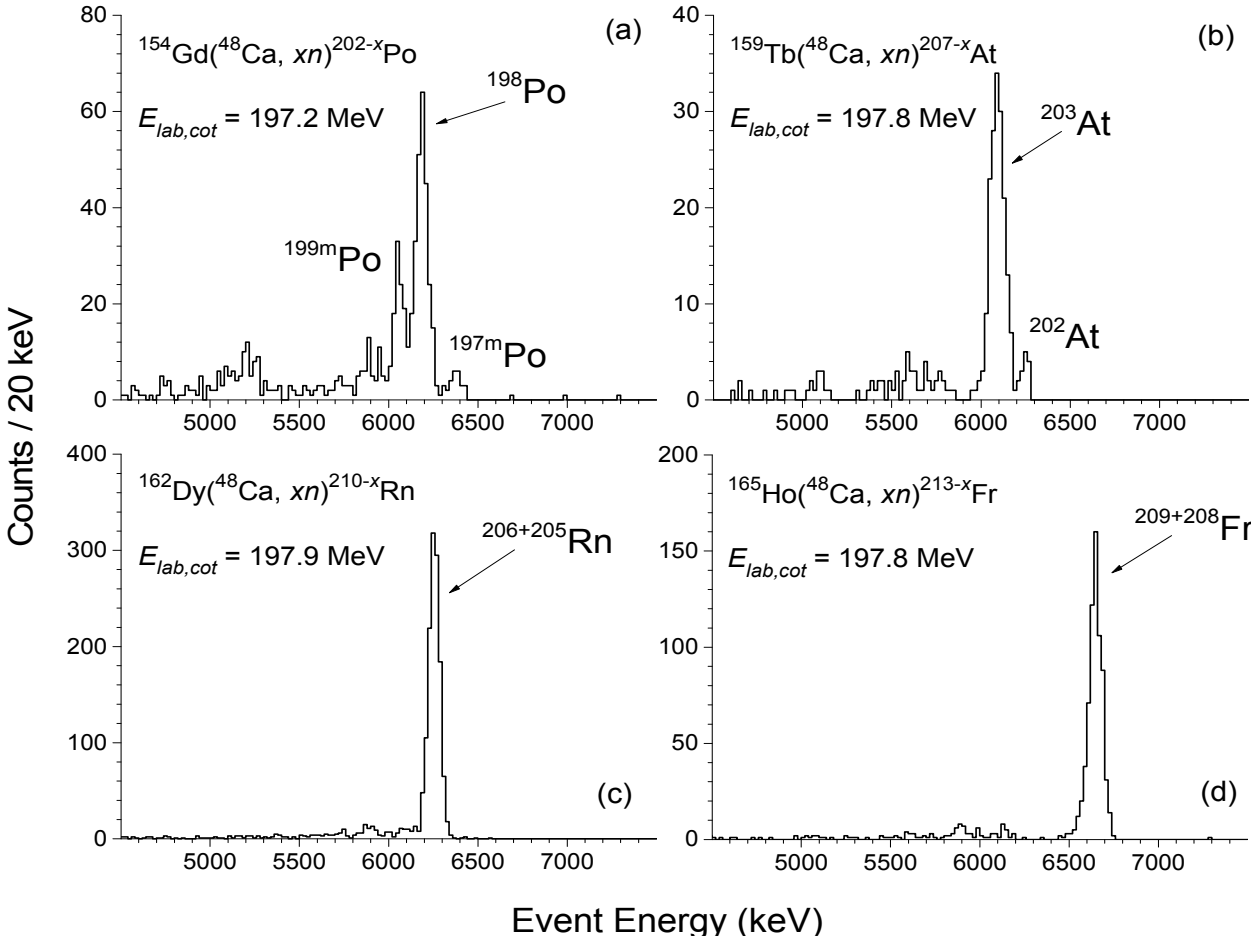

FIG. 2 Typical alpha spectra for 4*n* EvRs produced in ^{48}Ca-induced reactions on (a) ^{154}Gd, (b) ^{159}Tb, (c) ^{162}Dy, and (d) ^{165}Ho. The laboratory-frame center-of-target energy corresponds to approximately the peak of the excitation function for each reaction for the 4*n* residues. The superscript "m" denotes a metastable state of the nuclide.

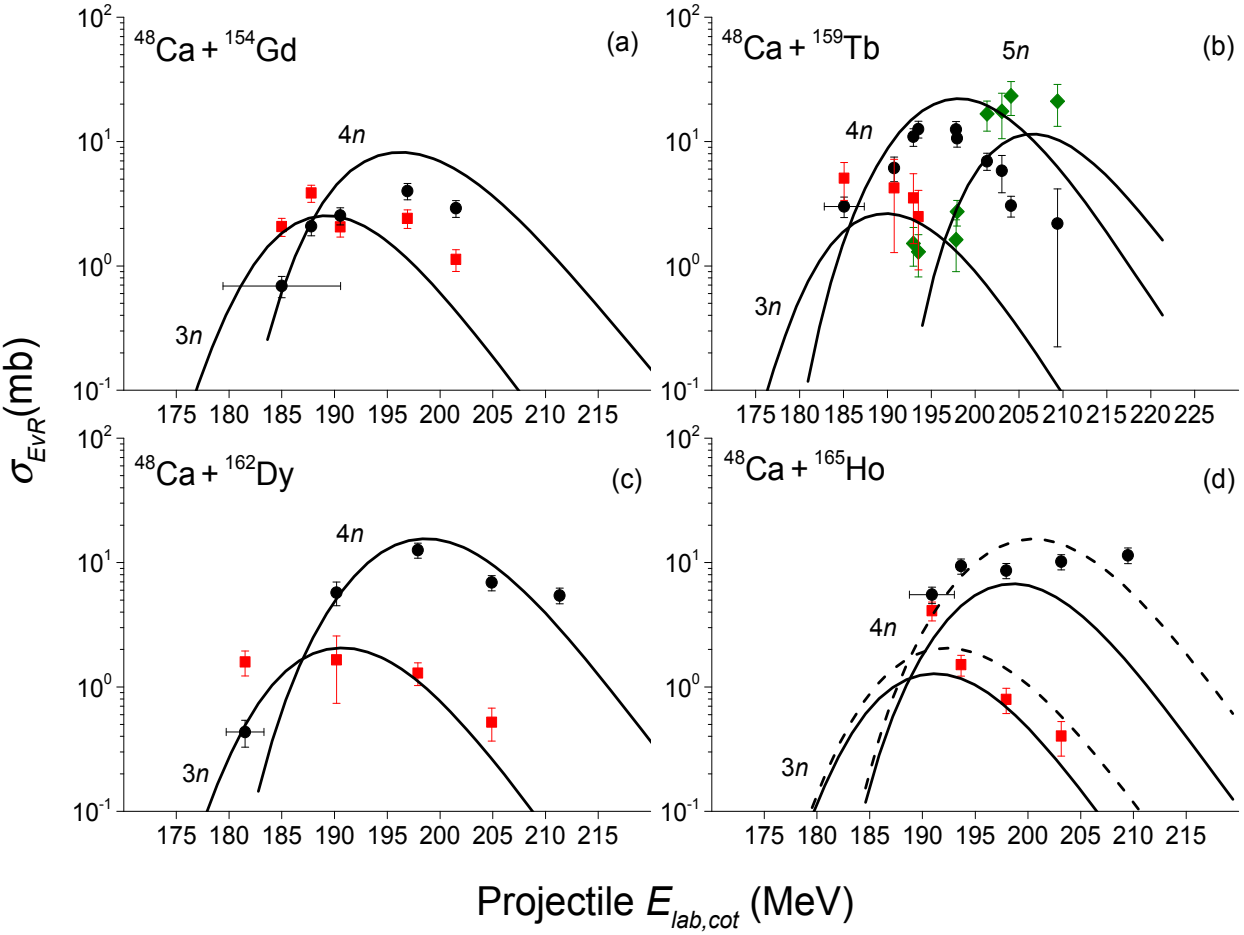

FIG. 3 (Color online) Excitation functions measured for ^{48}Ca-induced reactions on ^{154}Gd, ^{159}Tb, ^{162}Dy, and ^{165}Ho, showing the predominant evaporation channels for the studied projectile energy range. Solid lines correspond to model calculations discussed in Section IV, with the dashed curves in panel (d) calculated with an adjusted LD fission barrier height (see the main text for details). Experimental data are also given in Table II. The rise of the high-energy side of the 4*n* excitation functions in (c) and (d) comes from the 5*n* EvRs, which share identical decay properties with the 4*n* EvRs.

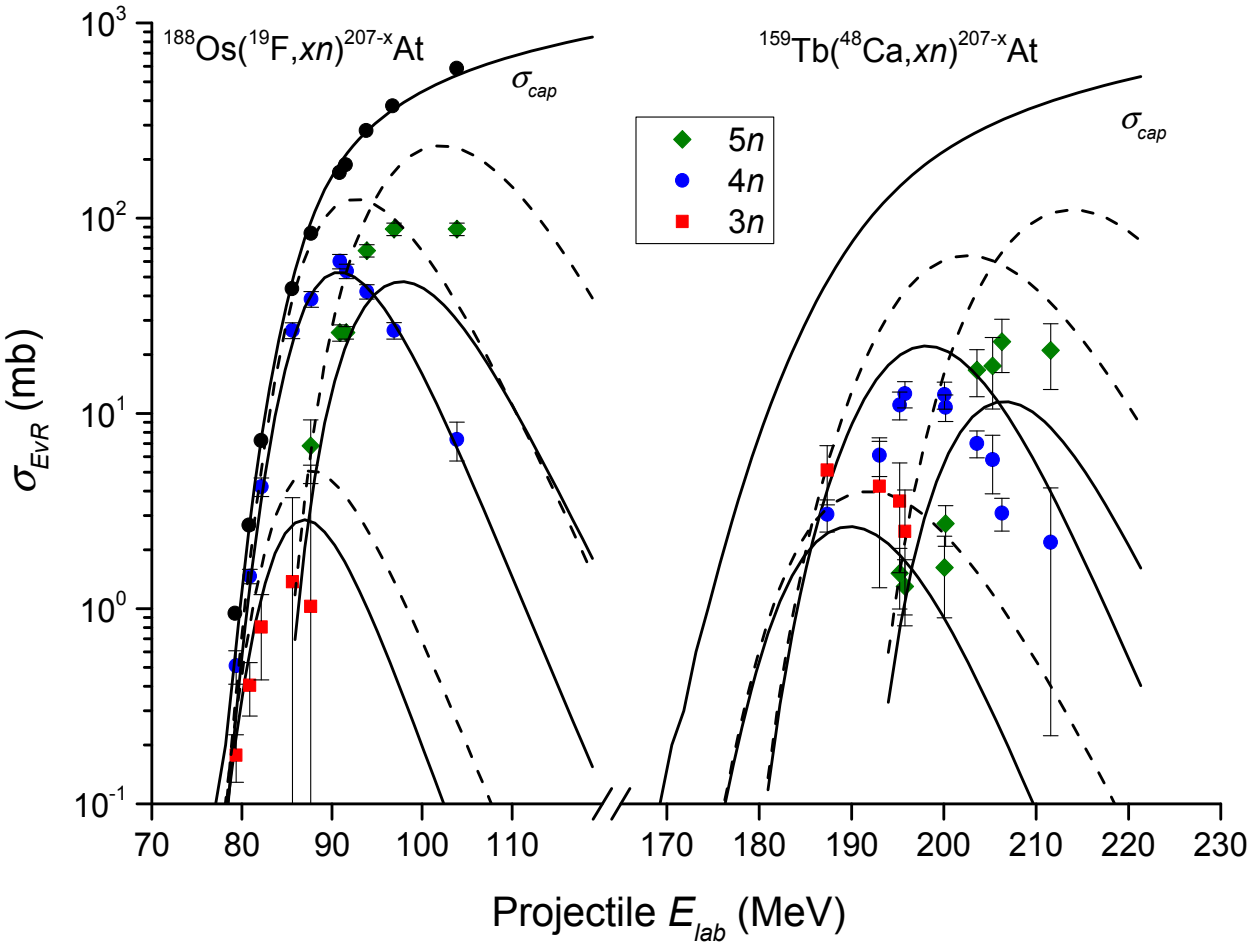

FIG. 4 (Color online) Excitation functions for production of $^{207-x}$At, where x is 3, 4, or 5, in the reactions ^{19}F + ^{188}Os and ^{48}Ca + ^{159}Tb. The capture cross section is labeled by σ_{cap}. Experimental data are shown by points; curves correspond to model calculations discussed in Section IV. Solid curves are calculations with CELD, and dashed curves are calculations without CELD.

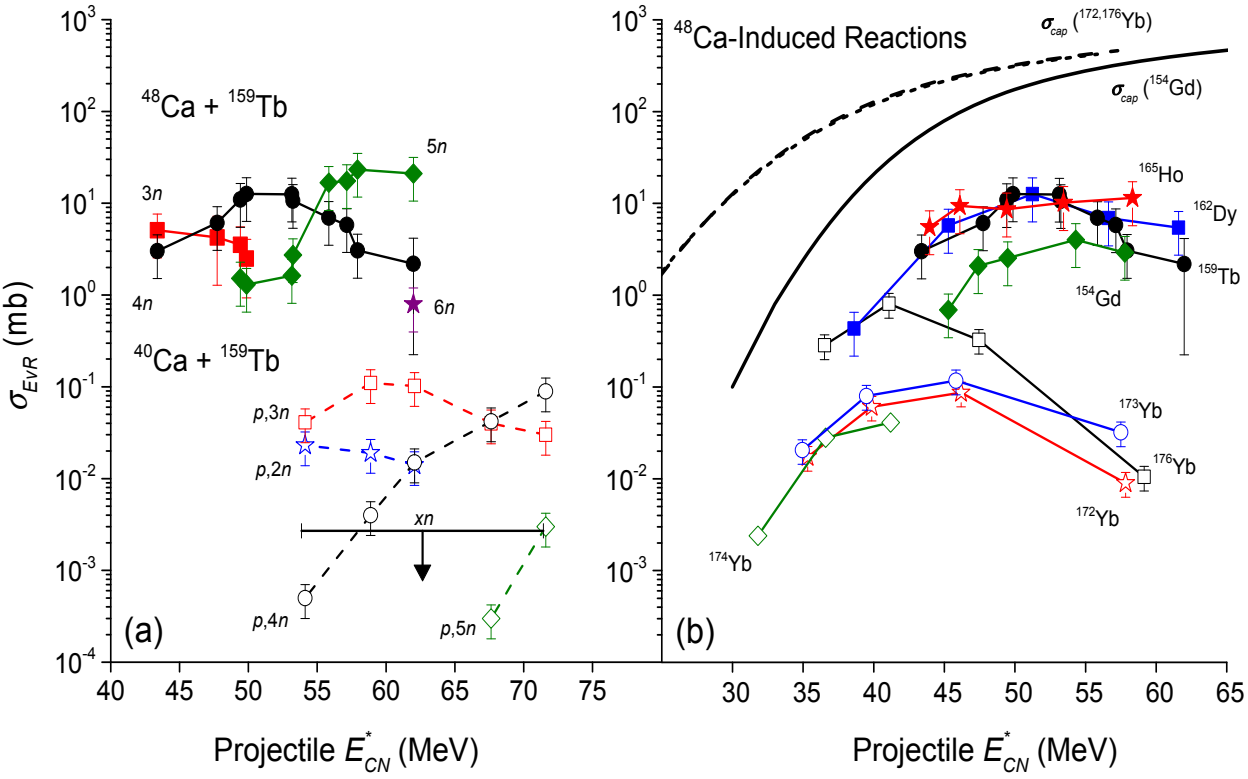

FIG. 5 (Color online) Excitation functions for reactions of ^{40,48}Ca with lanthanide targets. In (a), present ^{48}Ca + ^{159}Tb data is compared to ^{40}Ca + ^{159}Tb measurements from Ref. [2]. The arrow marks the maximum cross section measured for the *xn* EvRs in the ^{40}Ca reaction. In (b), 4*n* excitation functions for reactions of ^{48}Ca on ^{154}Gd, ^{159}Tb, ^{162}Dy, and ^{165}Ho studied in the present work, and $^{176,174\text{-}172}$Yb [5, 49] are compared. Calculated σ_{cap} for ^{48}Ca + ^{154}Gd, ^{48}Ca + ^{176}Yb, and ^{48}Ca + ^{172}Yb are shown by solid, dashed, and short-dashed curves, respectively. The reported error bars in case of the ^{174}Yb target are smaller than the data points. The remaining error bars represent absolute uncertainties.